

The first cyclotron harmonic of 4U 1538–52

J. J. Rodes-Roca^{1,2}, J. M. Torrejón¹, I. Kreykenbohm^{3,4}, S. Martínez Núñez¹, A. Camero-Arranz⁵ and G. Bernabéu¹

¹ Department of Physics, Systems Engineering and Sign Theory, University of Alicante, 03080 Alicante, Spain
e-mail: rodes@dfists.ua.es

² Department of Physics and Astronomy, University of Leicester, Leicester, LE1 7RH, UK

³ Dr. Karl Remeis-Sternwarte, Sternwartstr. 7, D-96049 Bamberg, Germany

⁴ Erlangen Centre for Astroparticle Physics (ECAP), Erwin-Rommel-Str. 1, 91058 Erlangen, Germany

⁵ National Space Science and Technology Center, 320 Sparkman Drive, Huntsville, AL 35805, USA*

Received ; accepted

ABSTRACT

Context. Cyclotron resonant scattering features are an essential tool for studying the magnetic field of neutron stars. The fundamental line provides a measure of the field strength, while the harmonic lines provide information about the structure and configuration of the magnetic field. Until now only a handful of sources are known to display more than one cyclotron line and only two of them have shown a series of harmonics.

Aims. The aim of this work is to see the first harmonic cyclotron line, confirming the fundamental line at ~ 22 keV, thus increasing the number of sources with detected harmonic cyclotron lines.

Methods. To investigate the presence of absorption or emission lines in the spectra, we have combined *RXTE* and *INTEGRAL* spectra. We modeled the 3–100 keV continuum emission with a power law with an exponential cut off and look for the second absorption feature.

Results. We show evidence of an unknown cyclotron line at ~ 47 keV (the first harmonic) in the phase-averaged X-ray spectra of 4U 1538–52. This line is detected by several telescopes at different epochs, even though the S/N of each individual spectrum is low.

Conclusions. We conclude that the line-like absorption is a real feature, and the most straightforward interpretation is that it is the first harmonic, thus making 4U 1538–52 the fifth X-ray pulsar with more than one cyclotron line.

Key words. X-rays: binaries – stars: pulsars: individual: 4U 1538–52

1. Introduction

Cyclotron resonant scattering features (CRSFs), usually referred to as ‘cyclotron lines’, have proved to be powerful tools for directly studying the magnetic field in neutron stars. CRSFs are present in the hard X-ray spectra of several X-ray pulsars and originate in the “cyclotron process” under extreme conditions. Through $E_{\text{cyc}} = 11.6B_{12} \times (1+z)^{-1}$ keV (the ‘12-B-12 law’, where z is the gravitational redshift), an energy of the fundamental feature in the hard X-rays indicates that the magnetic fields are rather strong ($B \sim 10^{12}$ G). Under such conditions, the interaction of the electrons and radiation must be treated quantum-mechanically. The behaviour of an electron in a strong magnetic field implies that the electron energy must be quantized in so-called Landau levels. These absorption features stem from the resonant scattering of photons by electrons, also referred to as cyclotron lines.

While the fundamental energy of the cyclotron line provides valuable information about the magnitude of the field, it is only through the detection and the analysis of the harmonic lines that we can get direct information about the geometrical configuration of the B field (Harding & Daugherty

1991; Araya-Góchez & Harding 2000; Schönherr et al. 2007). However, to date, only in a handful of systems have harmonic lines been discovered, and only two systems have shown more than two (Santangelo et al. 1999 & Coburn et al. 2005). It is therefore paramount to add as many systems to this selected group as we can.

In this work, we present a spectral analysis of the high mass X-ray binary pulsar 4U 1538–52. It is an eclipsing system consisting of the B0 I supergiant star QV Nor and a neutron star with an orbital period of ~ 3.728 days (Clark 2000). The orbital eccentricity is ~ 0.08 (Corbet et al. 1993), although more recently a higher value of ~ 0.17 was deduced by Clark (2000). The X-ray eclipse lasts ~ 0.6 days (Becker et al. 1977). The system is fairly bright in X-rays. The estimated flux is $\sim (5 - 20) \times 10^{-10}$ erg $\text{s}^{-1} \text{cm}^{-2}$ in the 3–100 keV range (Rodes 2007). Thus, assuming a distance of the source of ~ 5.5 kpc (Becker et al. 1977, Parkes et al. 1978) and an isotropic emission, the luminosity follows $\sim (2 - 7) \times 10^{36}$ erg/s. The magnetized neutron star has a spin period of ~ 529 s (Davison 1977; Becker et al. 1977).

The pulse-phase averaged X-ray spectrum of 4U 1538–52 has usually been described either by an absorbed power law modified by a high energy cutoff, a power law modified by a Fermi-Dirac cutoff, or by two power laws with indices of opposite sign multiplied by an exponential cutoff (the NPEX model, Mihara 1995; Rodes et al. 2006). In addition to these continuum models, an iron fluorescence line at ~ 6.4 keV and a cyclotron

Send offprint requests to: J. J. Rodes

* Fundación Española de Ciencia y Tecnología, C/ Rosario Pino, 14-16, 28020 Madrid, Spain

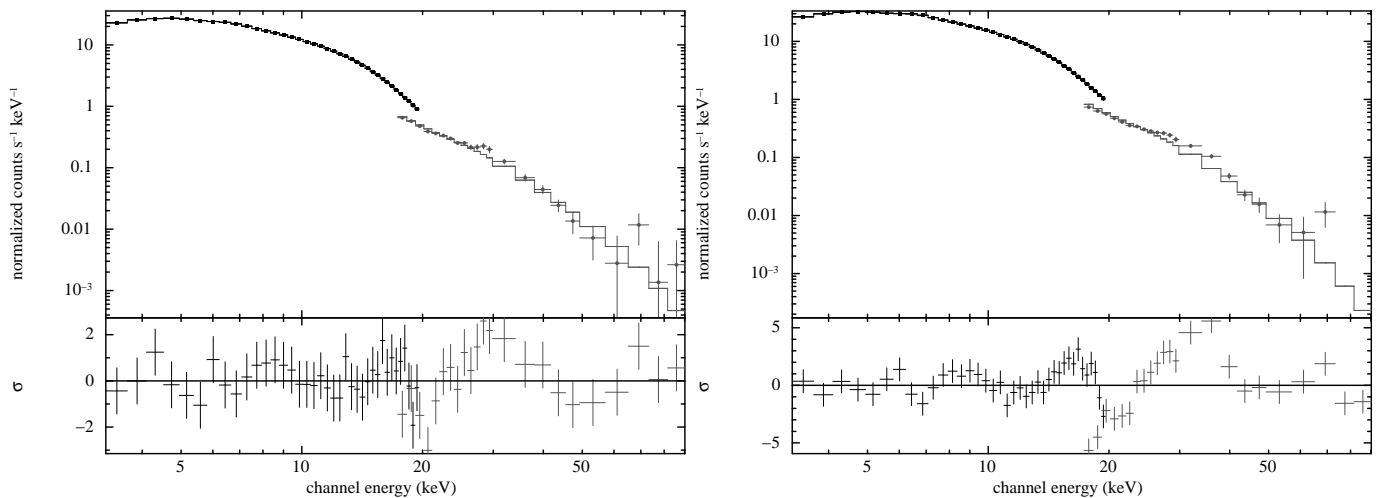


Fig. 1. Combined spectrum and model of data obtained with *PCA* (3–20 keV) and *HEXTE* (17–100 keV). Both data sets belong to the run carried out in 2001 and their orbital phases are 0.53 and 0.66, respectively. Bottom panels show the residuals in units of σ with respect to the model (see Section 3.1 for details).

resonant scattering feature at ~ 20 keV discovered by *Ginga* (Clark et al. 1990) are needed to describe the data. The variability of this CRSF was studied by Rodes-Roca et al. (2008). Rossi X-ray Timing Explorer (*RXTE*) (Coburn 2001) and *BeppoSAX* data (Robba et al. 2001) did not show evidence of the first harmonic at ~ 40 keV. Robba et al. (2001) presented some evidence of an absorption feature around 50 keV; however, because of the lack of a signal-to-noise ratio of the spectrum at these energies, the feature could not be confirmed.

In this paper, we report on the 3–100 keV analysis based on the observations of 4U 1538–52 performed by the *RXTE* and *INTEGRAL* satellites. In Sect. 2 we describe the observations and data analysis. In Sect. 3 spectral analysis are presented, and summarized in Sect. 4.

2. Observations

2.1. *RXTE* data

To study the presence of spectral features, we have used all archival data from *RXTE* on this source: three observations have been carried out in 1996, 1997, and 2001. The first one, is a monthly observation between 1996 November 24 and 1997 December 13. The second and third ones cover a complete orbital period. In our analysis we used data from both *RXTE* pointing instruments, the Proportional Counter Array (*PCA*) and the High Energy X-ray Timing Experiment (*HEXTE*).

To extract the spectra, we used the standard *RXTE* analysis software *FTOOLS*¹. This package takes care of the modeling of *PCA* background, the dead time corrections of *HEXTE* data and generates the appropriate response matrices for the spectral analysis.

The *PCA* consists of five co-aligned Xenon proportional counter units with a total effective area of ~ 6000 cm² and a nominal energy range from 2 keV to over 60 keV (Jahoda et al. 1996). However, because of response problems above ~ 20 keV and the Xenon-K edge around 30 keV, we restricted the use of the *PCA* to the energy range from 3 keV to 20 keV (see also Kreykenbohm et al. 2002). Systematic uncertainties are taken into account by the standard spectral analysis.

The *HEXTE* consists of two clusters of four NaI(Tl)/CsI(Na) Phoswich scintillation detectors with a total net detector area of 1600 cm². These detectors are sensitive from 15 keV to 250 keV (Rotschild et al. 1998), however, response matrix, instrument background and source count rate, limit the energy range from 17 to 100 keV. Background subtraction in *HEXTE* is done by source-background swapping of the two clusters every 32 s throughout the observation. For the *HEXTE*, the response matrices were generated with *HXTRSP*, version 3.1. We used *HXTDEAD* version 2.0.0 to correct for the dead time. In order to improve the statistical significance of the data, we added the data of both *HEXTE* clusters and created an appropriate response matrix by using a 1:0.75 weighting to account for the loss of a detector in the second cluster. We also binned several channels together of the *HEXTE* data at higher energies and chose the binning as a compromise between increased statistical significance while retaining a reasonable energy resolution.

2.2. *INTEGRAL* data

INTEGRAL (Winkler et al. 2003) has a unique broad band capability thanks to its four science instruments (imager *IBIS*, spectrometer *SPI*, X-ray monitor *JEM-X*, and optical monitor *OMC*) which allow us to study a source from 3 keV up to 10 MeV and in the optical simultaneously. The imager *IBIS* has a very large field of view of $9^\circ \times 9^\circ$ which allows us to observe many sources at the same time. Together with a large collecting area of 2600 cm² and decent energy resolution of 9% at 100 keV makes *IBIS* the prime instrument for our analysis.

Since its launch on October 17 2002, *INTEGRAL* observatory has been constantly collecting a wealth of data. *INTEGRAL* data are organized in revolutions (i.e. 72 h long satellite orbits around the Earth) and then science windows which are typically 1800 s to 3600 s long.

The source was observed by the hard X-ray imager (*IBIS*) camera on board *INTEGRAL* during the regular scans of the Galactic plane and the Norma survey. Fig. 2 shows an *IBIS/ISGRI* mosaic image of the Norma Arm region in the energy range 20–100 keV. The source 4U 1538–52 (labelled as H 1538–522) is clearly detected and its position is well determined, allowing us to extract its spectrum without contamination of other sources in the field of view of the instrument.

¹ available at <http://heasarc.gsfc.nasa.gov>

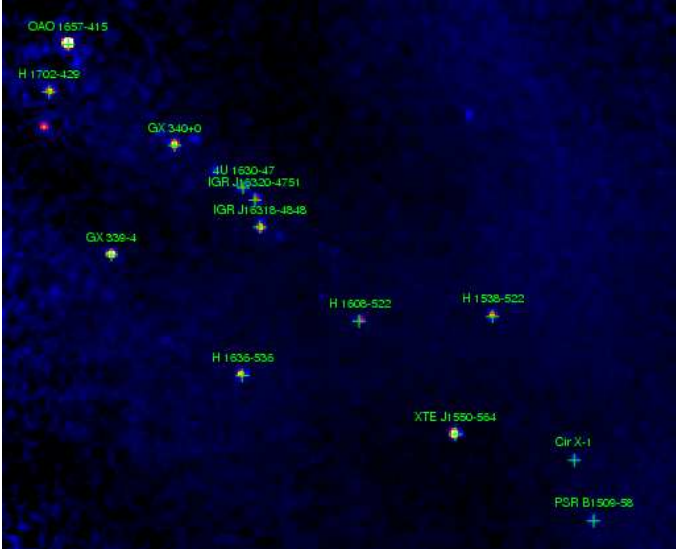


Fig. 2. *IBIS/ISGRI* mosaic image of the Norma Arm region where the source is located and clearly detected.

Table 1. Details of observations.

Satellite/Instrument	MJD	Exposure (ks)	Orbital phase
RXTE/PCA	51925.25	9.296	0.53
RXTE/HEXTE	51925.25	6.418	0.53
RXTE/PCA	51925.74	12.592	0.66
RXTE/HEXTE	51925.74	8.261	0.66
INTEGRAL/ <i>JEM-X</i> 1	53407.7–53826.3	360	
INTEGRAL/ <i>ISGRI</i>	52651.4–53756.2	720	
INTEGRAL/ <i>SPI</i>	52651.4–53941.4	1907	

To extract *INTEGRAL* data, we used the Offline Science Analysis Software (OSA) version 7.0, as distributed by the Integral Science Data Centre (ISDC) following the respective cookbook² instructions. For *IBIS*, we selected all public data up to revolution 400 with the source in the fully coded field of view of the instrument, resulting in ~ 400 Science Windows (ScWs). In a first step we created a mosaic of the full data set to obtain a catalog of the detected sources in the field of view. Since 4U 1538–522 is relatively close to the galactic centre, the catalog contains other 15 sources, among them several bright sources such as 4U 1700–377. We then used this catalog to extract the spectrum of 4U 1538–522 using all 400 ScWs in order to obtain a high signal-to-noise ratio. Since all other sources in the field are several degrees away, source confusion is not a problem. For *JEM-X* we used all data of monitor number one (*JEM-X* 1) within 2° to ensure a reliable spectrum resulting in approximately 55 ScWs. And for *SPI*, the selection of all available data within a 8° radius (the fully coded field of view of the instrument) allowed us to obtain 969 ScWs. The selected spectra then have an effective exposure time of 720 ksec for *IBIS*, 1907 ksec for *SPI*, and 360 ksec for *JEM-X*.

See Table 1 for the details of all observations which have been used in this work.

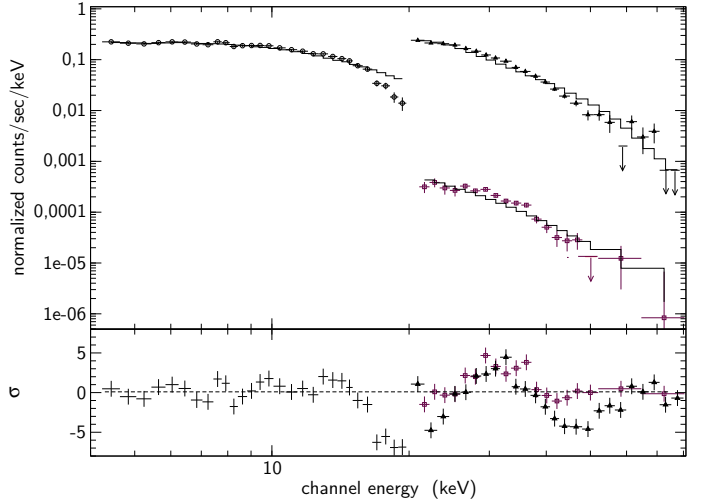


Fig. 3. Combined spectrum and model obtained with *JEM-X* (left), *ISGRI* (upper right), and *SPI* (lower right). The continuum is modeled by the *CUTOFFPL* model without any cyclotron lines applied. The bottom panel shows the residuals in units of σ with respect to the model. The first harmonic at ~ 47 keV is already evident in the raw data.

3. Spectral analysis

For spectral analysis we used the *XSPEC* (Arnaud 1996) fitting package, released as a part of *XANADU* in the *HEASoft* tools.

3.1. *RXTE* analysis

Fig. 1 shows *PCA* and *HEXTE* phase-averaged spectrum at orbital phases 0.53 (left panel) and 0.66 (right panel). The raw data together the best-fit model and the residuals of the fit as the difference between observed flux and model flux divided by the uncertainty of the observed flux, i. e. in units of σ , are included in this plot. The dip of the second cyclotron line at ~ 47 keV is apparent in the raw data. The *RXTE* continuum is properly described by an absorbed powerlaw modified by an exponential cutoff at $E_{\text{cut}} = 9.4^{+1.1}_{-0.23}$ keV (*CUTOFFPL* in *XSPEC* (Arnaud 1996)), see Table 2. Analytically, *CUTOFFPL* is given by the equation,

$$\text{cutoffpl}(E) = K (E/1\text{keV})^{-\alpha} e^{-E/E_{\text{cut}}}, \quad (1)$$

where α is the power law photon index and E_{cut} is the cutoff energy in keV. An iron emission line at 6.4 keV was also added. The proper description of the continuum, however, further required a very broad Gaussian emission line component at 12 keV to account for a flux excess at these energies. This phenomenological component has been used to describe the continuum of several X-ray pulsars (Coburn et al. 2002 concluded that this bump is an inherent feature in the spectra of accreting pulsars). Although it has no clear physical interpretation, its use here is justified as we concentrate on the presence of absorption features at significantly higher energies. See Table 2 for the best fit spectral parameters for the data set in Fig. 1. Data from *PCA* and *HEXTE* have been fitted simultaneously. All uncertainties refer to a single parameter at the 90% ($\Delta\chi^2 = 2.71$) confidence limit³.

A significant absorption feature is present in the residuals around ~ 47 keV. When other models are used to describe the

² available at <http://isdc.unige.ch>

³ Also in Tables 3, 4 and 5

Table 2. Fitted parameters for the *RXTE* spectra in Fig. 1.

Component	Parameter	Left panel	Right panel
Continuum	α	$0.74^{+0.18}_{-0.14}$	0.52 ± 0.11
	E_{cut} (keV)	$11.4^{+2.0}_{-1.2}$	$9.4^{+1.1}_{-0.23}$
	N_H (10^{22} cm $^{-2}$)	$1.0^{+0.6}_{-0.5}$	$1.05^{+0.10}_{-0.20}$
Gaussian emission line	E_{bump} (keV)	$12.54^{+0.21}_{-0.3}$	$12.15^{+0.10}_{-0.09}$
	σ_{bump} (keV)	$3.12^{+0.22}_{-0.23}$	$2.92^{+0.08}_{-0.12}$
Fluorescence iron line	E_{FeK} (keV)	$6.54^{+0.14}_{-0.11}$	$6.56^{+0.03}_{-0.14}$
	σ_{FeK} (keV)	$0.2^{+0.3}_{-0.19}$	0.1 (frozen)
	$\chi^2_r(\text{dof})$	1.2(51)	4.4(52)

Table 3. Fitted parameters for the *INTEGRAL* spectrum in Fig. 3.

Component	Parameter	
Continuum	α	0.29 ± 0.07
	E_{cut} (keV)	$9.06^{+0.22}_{-0.21}$
Normalization	C_{JEM-X}	0.90 ± 0.03
	C_{ISGRI}	1.0 (frozen)
	C_{SPI}	$1.29^{+0.08}_{-0.07}$
	$\chi^2_r(\text{dof})$	5.5(68)

underlying continuum, i.e. an absorbed powerlaw with a Fermi-Dirac cutoff (Tanaka 1986) or the NPEX model (Mihara 1995), the overall residuals were higher, but none of them was able to account for the absorption feature at ~ 47 keV.

3.2. INTEGRAL analysis

In Fig. 3, we present the combined *JEM-X*, *ISGRI* and *SPI* spectrum using all data. The spectra of all three instruments were fitted simultaneously with a `CUTOFFPL` model, using the latest response matrices provided by the OSA software (see Section 2.2 for more details). A factor term was included in the model to allow for the adjustment of efficiencies between different instruments. No photoelectric absorption has been used since the *INTEGRAL* spectra start only at 4 keV and none was required by the data. An absorption column below 10^{23} cm $^{-2}$ is expected to have no noticeable effect below 5 keV. Nevertheless *JEM-X* data are needed to constrain the X-ray continuum model. Likewise, neither the very broad Gaussian at 12 keV, nor the iron fluorescence line at 6.4 keV are required by the *JEM-X* data and were therefore not added to the model. As can clearly be seen in Fig. 3, significant absorption line structures are present at ~ 20 keV (the well known CRSF) and ~ 47 keV after fitting the continuum with a `cutoffpl` model (best-fit parameters of continuum are given in Table 3). Data from *JEM-X*, *ISGRI* and *SPI* have been fitted simultaneously.

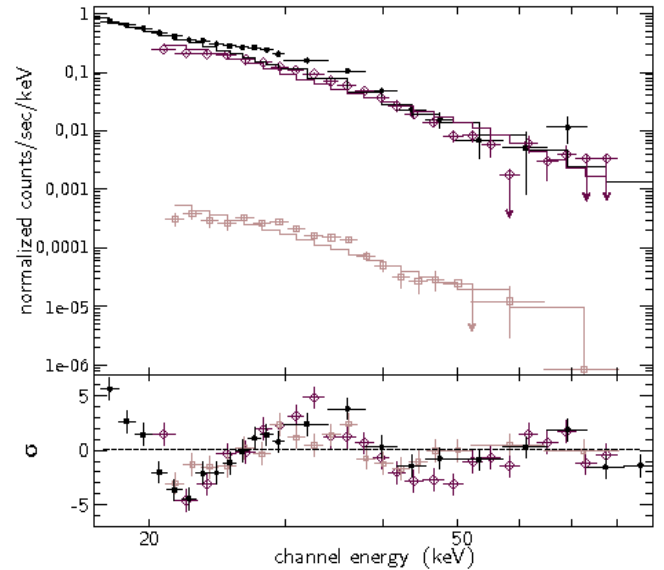
3.3. Combined RXTE and INTEGRAL analysis

To further explore this second feature and in order to achieve the highest significance at high energies, we jointly fitted the data of the high energy instruments of the two satellites, *HEXTE*, *ISGRI*, and *SPI*. We fixed the continuum parameters α , the power law photon index and E_{cut} , the cutoff energy of the exponential cutoff, to the values given in Table 3.

Table 4. Fitted parameters for the fundamental and the first harmonic CRSF.

Parameter	<i>SPI</i>	<i>ISGRI</i>	<i>HEXTE</i>
Fundamental			
E_{c1} (keV)	$22.7^{+0.9}_{-2.4}$	$22.0^{+1.0}_{-1.6}$	$20.7^{+1.3}_{-3}$
τ_{c1}	$0.8^{+0.4}_{-0.3}$	$0.5^{+1.6}_{-0.18}$	$0.5^{+1.3}_{-0.13}$
σ_{c1} (keV)	$3^{+4}_{-1.7}$	3^{+5}_{-2}	4^{+6}_{-3}
1 st Harmonic			
E_{c2} (keV)	$42^{+4}_{-1.5}$	47^{+3}_{-10}	48^{+9}_{-7}
τ_{c2}	$0.9^{+1.0}_{-0.5}$	$0.8^{+0.5}_{-0.21}$	$0.6^{+1.7}_{-0.3}$
σ_{c2} (keV)	$3^{+11}_{-1.9}$	10^{+22}_{-6}	8^{+24}_{-7}
$\chi^2_r(\text{dof})$	1.0(14)	1.1(18)	0.8(16)

In Table 4 we show the best fit parameters for each spectrum we used in Fig. 4. Data from *SPI*, *ISGRI* and *HEXTE* have been fitted individually. As the continuum parameters are frozen, we have not included them in this Table. The results of the spectral fits from three different instruments show that the values describing the *shape* of the cyclotron lines are consistent with one to another within uncertainties.

**Fig. 4.** Spectra and continuum model (`cutoffpl`) obtained with *ISGRI*, *SPI* (lower), and *HEXTE*. The bottom panel shows the residuals in units of σ of a fit without including a cyclotron line.

As evident from Fig. 4, the two cyclotron absorption features are clearly seen in the raw data of the three instruments. Although *SPI* has a very high energy resolution, the compared to *ISGRI* rather low signal-to-noise ratio required the use of rather broad energy bins. Therefore we will use *ISGRI* as the prime instrument in our study together with *HEXTE* while *SPI* data will be used for comparison. In summary, to get the best fit parameters of the absorption features, we have combined *ISGRI* and *HEXTE* data including a factor for free normalization between the two instruments (see Fig. 5 top panel). The two absorption features at ~ 22 keV and ~ 47 keV are modeled using the `CYCLABS` model from XSPEC (Arnaud 1996).

We started by modeling the fundamental cyclotron line that was discovered by the *Ginga* satellite observatory (Clark et al. 1990) (see Fig. 5 second panel). After the inclusion of the

Table 5. Best fit parameters for the fundamental and the first harmonic CRSF.

Component	Parameter	
Continuum	α	0.29 (frozen)
	E_{cut} (keV)	9.1 (frozen)
Fundamental	E_{c_1} (keV)	$21.4^{+0.9}_{-2.4}$
	τ_{c_1}	$0.43^{+0.3}_{-0.07}$
	σ_{c_1} (keV)	3^{+4}_{-2}
1 st Harmonic	E_{c_2} (keV)	$47.1^{+2.2}_{-1.7}$
	τ_{c_2}	$0.88^{+0.5}_{-0.24}$
	σ_{c_2} (keV)	$5^{+5}_{-2.3}$
$\chi^2_v(\text{dof})$		1.4(41)

fundamental cyclotron line at $E \sim 21.4$ keV, the χ^2_v improves from 5.5 for 47 degrees of freedom (dof) to 3.4, for 44 dof (F-test: 3.0×10^{-5}). Although residuals improve significantly (see Fig. 5 third panel), another absorption feature can be seen at ~ 47 keV. Including a second cyclotron line at ~ 47 keV improves the fit further resulting in a χ^2_v of 1.4 for 41 dof (F-test: 1.7×10^{-8} see Fig. 5 bottom panel). *ISGRI* data (filled grey circles in Fig. 5) has a far better resolution than *HEXTE* at these energies. However, the overall shape is virtually identical, ruling out any instrumental or circumstantial effects. The final fit parameters are given in Table 5. Data from *HEXTE* and *ISGRI* have been fitted simultaneously.

The F-test is known to be problematic when used to test the significance of an additional spectral feature (see Protassov & van Dik 2002), even if systematic uncertainties are not an issue. However, the low false alarm probabilities may make the detection of the line stable against even crude mistakes in the computation of the significance (Kreykenbohm 2004). Therefore, taking into account these caveats, we can conclude that the the first harmonic CRSF is detected with high significance in the spectrum of this source.

Although the uncertainties of the determined values are rather large, these values are consistent with one another within uncertainties. This makes it extremely unlikely that the ~ 47 keV feature results from a calibration problem. Nevertheless, the line parameters depend slightly on the shape of the continuum (for example, using the NPEX component (Mihara 1995) and two cyclotron absorption lines, we obtained the line centre energies at ~ 22 keV and ~ 44 keV, for the fundamental and first harmonic respectively).

In short, this feature has been found to be present under the following circumstances:

- Three different telescopes and instruments: Narrow Field Instruments (*NFIs*) on board *BeppoSAX* (Robba et al. 2001), *HEXTE* on board *RXTE*, and *IBIS/ISGRI* on board *INTEGRAL* (this work).
- Different epochs within the same telescope (i.e. 1996, 1997, 2001 using *RXTE*).
- Different orbital phases within a given epoch and instrument (Fig. 1).

We therefore conclude, that despite the relatively low significance of the feature in an *individual* observation, its detection in different epochs, configuration of the binary system, and different instrumentation, makes this feature highly significant. The most direct explanation for this absorption line like feature is that it is the first harmonic cyclotron line.

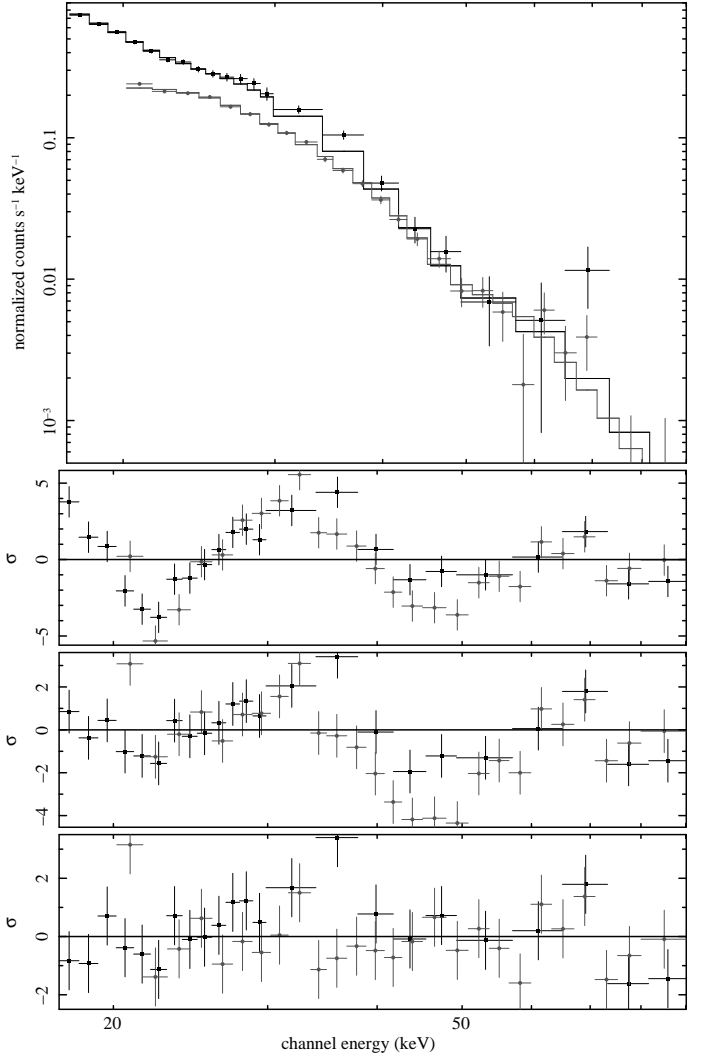


Fig. 5. Cyclotron line modeling of the phase-averaged spectra *HEXTE/ISGRI* of 4U 1538–52. *Top panel:* Spectra and best fit model (cutoffpl and two cyclotron lines) obtained with *HEXTE* and *ISGRI*. *Bottom panels* show the residuals in units of σ for models taking different numbers of cyclotron lines into account. *Second panel:* Without cyclotron lines. *Third panel:* Fundamental cyclotron line at ~ 22 keV. *Bottom panel:* Two cyclotron lines, the fundamental at ~ 22 keV and the first harmonic ~ 47 keV (see Table 5 for the best fit values).

4. Summary and discussion

We presented the spectral analysis of 4U 1538–52 using data from *RXTE* and *INTEGRAL*. We present evidence for a previously unknown absorption line like feature in the phase-averaged spectrum of the source. As we have shown in Section 3, we have been able to achieve a good fit to the phase-averaged spectra by including a Lorentzian absorption line at ~ 47 keV into the model (see Fig. 5). This absorption line is clearly visible whenever the signal-to-noise ratio in the spectrum is good enough to allow an analysis of the data. The most straightforward interpretation for this feature is that it is the first harmonic of the ~ 22 keV fundamental CRSF.

According to the theory, cyclotron lines are due to the resonant scattering of photons by electrons whose energies are quantized into Landau levels by the magnetic field (Mészáros 1992). The quantized energy levels of the electrons are harmon-

ically spaced in the first order, such that the first harmonic line should be placed at twice the energy of the fundamental line, i.e. $2 \times E_{\text{cyc}} \approx 42$ keV. In reality, however, the coupling factor between the fundamental and first harmonic is with ~ 2.20 slightly higher than 2.0. This anharmonic spacing, however, has been observed already in several systems where more than one line is present. As explained by Schönherr et al. (2007), the relativistic photon-electron scattering already produces some anharmonicity, because photons with energies close to the Landau levels may not escape the plasma if their energies are not changed by inelastic scattering. This, however, can not be the only reason because some systems show an anharmonic spacing larger than that predicted by this effect. A possibility to explain this difference is to take into account that the optical depths of the fundamental and the first harmonic could be different if they are formed at different heights above the neutron star. With increasing height, the strength of the magnetic field decreases resulting in a different CRSF energy. Another possibility is to consider a displacement of the magnetic dipole which would also explain the difference of energy of the two lines if the lines originate from the different poles of the neutron star. Therefore a significant phase dependence of the strength of the both lines is expected, however, the low signal-to-noise ratio at higher energies prevents us to test this hypothesis with the current data sets.

Acknowledgements. We are grateful to the anonymous referee for useful and detailed comments. Part of this work was supported by the Spanish Ministry of Education and Science *Primera ciencia con el GTC: La astronomía española en vanguardia de la astronomía europea* CSD200670 and *Multiplidad y evolución de estrellas masivas* project number AYA200806166C0303. This research has made use of data obtained through the High Energy Astrophysics Science Archive Research Center Online Service, provided by the NASA/Goddard Space Flight Center and through the INTEGRAL Science Data Center (ISDC), Versoix, Switzerland. SMN is a researcher of the Programme Juan de la Cierva, funded by the MICINN. JMT acknowledges the support by the Spanish Ministerio de Educación y Ciencia (MEC) under grant PR2007-0176. ACA thanks for the support of this project to the Spanish Ministerio de Ciencia e Innovación through the 2008 postdoctoral program MICINN/Fulbright under grant 2008-0116. JJRR acknowledges the support by the Spanish Ministerio de Educación y Ciencia (MEC) under grant PR2009-0455.

References

- Araya-Góchez, R. A. & Harding, A. K. 2000, *ApJ*, 544, 1067
- Arnaud, K. A. 1996, in *Astronomical Data Analysis Software and Systems V*, ed. J. H. Jacoby & J. Barnes, ASP Conf. Ser. 101, San Francisco, 17.
- Becker, R. H., Swank, J. H., Boldt, E. A. et al. 1977, *ApJ*, 216, L11
- Bulik, T., Riffert, H., Mészáros, P. et al. 1995, *ApJ*, 444, 405
- Clark, G. W., Woo, J. W., Nagase, F. et al. 1990, *ApJ*, 353, 274
- Clark, G. W. 2000, *ApJ*, 542, L131
- Coburn, W. 2001, Ph. D. thesis, University of California, San Diego
- Coburn, W., Heindl, W. A., Rothschild, R. E., et al. 2002, *ApJ*, 580, 394
- Coburn, W., Kretschmar P., Kreykenbohm, I., et al. 2005, *ATel*, 381, 1
- Corbet, R. H. D., Woo, J. W. & Nagase, F. 1993, *A&A*, 276, 52
- Davison, P. J. N., Watson, M. G. & Pye, J. P. 1977, *MNRAS*, 181, 73P
- Harding, A. K. & Daugherty, J. K. 1991, *ApJ*, 374, 687.
- Jahoda, K., Swank, J. H., Giles, A. B. et al. 1996, in *EUV, X-ray and Gamma-Ray Instrumentation for Astronomy VII Proc. SPIE*, ed. O. H. Siegmund & M. A. Gummin, vol. 2808, SPIE, 59
- Kreykenbohm, I. 2004, Ph. D. thesis, University of Tübingen
- Kreykenbohm, I., Coburn, W., Wilms, J. et al. 2002, *A&A*, 395, 129
- Mészáros, P. 1992, *High-energy radiation from magnetized neutron stars*, University of Chicago Press
- Mihara, T. 1995, Ph.D. thesis, University of Tokyo
- Parkes, G. E., Murdin, P. G. & Mason, K. O. 1978, *MNRAS*, 184, 73P
- Protassov, R. & van Dik, D. A. 2002, *ApJ*, 571, 545
- Robba, N. R., Burderi, L., Di Salvo, T. et al. 2001, *ApJ*, 526, 950
- Rodes, J. J., Torrejón, J. M. & Bernabéu, G. 2006, in *The Many Scales in the Universe*, ed. J. C. del Toro Iniesta, E. J. Alfaro, J. G. Gorgas, E. Salvador Solé & H. Butcher
- Rodes, J. J. 2007, Ph.D. thesis, University of Alicante
- Rodes-Roca, J. J., Torrejón, J. M. & Bernabéu, G. 2008, in *Lectures Notes and Essays in Astrophysics III*, ed. A. Ulla & M. Manteiga
- Rothschild, R. E., Blanco, P. R., Gruber, D. E. et al. 1998, *ApJ*, 496, 538
- Santangelo A., Segreto A., Giarrusso S. et al. 1999, *ApJ*, 523, L85
- Schönherr G., Wilms J., Kretschmar P. et al. 2007, *A&A*, 472, 353
- Tanaka, Y. 1986, in *Radiation Hydrodynamics in Stars and Compact Objects*, ed. Mihalas & K. H. A. Winkler (Springer Verlag), IAU Coll. 89, 198
- Wilms, J., Nowak, M. A., Dove, J. B. et al. 1999, *ApJ*, 522, 460
- Winkler, C., Courvoisier, T. J.-L., Di Cocco, G., et al. 2003, *A&A*, 411, L1